JOURNAL OF AIRCRAFT
Vol. 45, No. 1, January–February 2008

Computational Fluid Dynamics Analysis of Externally Blown Flap Configuration for Transport Aircraft

H. A. Griffin,* L. F. Gonzalez,† and K. Shrinivas‡
University of Sydney, Sydney, New South Wales 2006, Australia

DOI: 10.2514/1.30842

As aircraft grow in size to meet the ever-increasing demand from the international traveling public, the limits imposed by current airport facilities become apparent. Continual growth of environmental awareness within the community and noise reduction requirements, combined with the issue of long takeoff and landing runs required by the large jet transport aircraft, create problems for engineers. The implementation of externally blown flaps would allow for steeper approach paths pertaining to a reduction in noise pollution and reduce the takeoff and landing distance required. The reduction in the distance required for aircraft operations will allow for an increase in the size of aircraft or operations from fields that were previously unavailable. The introduction of externally blown flaps has occurred on a production aircraft, the C-17 Globemaster III, in use with the United States Air Force. The advantages provided by the system are obvious, improving the aircraft's takeoff and landing performance dramatically. This study focuses on a computational fluid dynamics analysis of the three-dimensional flow characteristics of the externally blown flaps configuration for transport aircraft and future unmanned aerial vehicles operating in remote areas. The study compares two- and three-dimensional analysis with and without externally blown flaps, increasing understanding of the vital elements of the system so as to allow the possibility of further implementation of externally blown flaps in improving the airline industry in regard to airway congestion.

Nomenclature

C_D	=	coefficient of drag
C_L	=	coefficient of lift
C_p	=	coefficient of pressure
k-ω	=	k-omega, turbulence model
k-ε	=	k-epsilon, turbulence model
Re	=	Reynolds number
U_9	=	engine exit core velocity
$U_{9'}$	=	engine bypass velocity
T_9	=	engine exit core temperature
$T_{9'}$	=	engine bypass temperature
α	=	angle of attack

I. Introduction

FROM the beginning of aircraft production, a compromise between different stages of flight has always existed, most notably the configuration changes that occur between the takeoff/landing and cruise segments of flight. As aircraft increase in size and payload capabilities, the methods of solving this problem of different flying speeds has become more complex. The introduction of flaps first began to aid in the reduction of airspeed for segments of flight without impacting upon the cruise efficiency of the aircraft. As aircraft became larger more complex, flap configurations were implemented along with leading-edge high-lift devices. Despite these advances in increasing the ability of an aircraft to fly at low speeds, takeoff and landing distances are still large and continue to grow with the ever-increasing size of modern aircraft [1]. The physical limits imposed by geographical locations combined with the modern public concern about aircraft noise requires improvements in high-lift devices to allow the use of shorter takeoff/landing runs and steeper approach paths.

Externally blown flaps (EBF) use engine exhaust to energize the flow over the flap, as shown in Fig. 1. In doing so, EBF increases the amount of lift produced by a wing that aids in the reduction of the takeoff/landing run required by an aircraft. The beneficial effects of EBF have been known since the 1970s, however, it has been possible only recently to include EBF on production aircraft [2]. The use of EBF also allows a steeper approach angle, meaning greater terrain clearance is possible, and a reduction in the area affected by aircraft noise. Both of these advantages would improve the operational abilities of aircraft, providing an increase in the number of airports that an aircraft could land at or, conversely, increasing the size of an aircraft without a subsequent increase in the landing/takeoff run which would remove the need for extended runways. The improvements in terrain clearance are most important in the military sector, whereas noise improvements, although not presently vital, may prove to provide a new standard that will be favorably accepted by the modern environmentally aware community.

A current application of EBF is the military transport aircraft produced by Boeing, C-17 Globemaster, which is the result of previous experimental work conducted by NASA in the 1970s [3]. The use of EBF on this aircraft has permitted extremely short takeoff and landing (STOL) capabilities, which allow the aircraft to perform unique missions into unprepared airfields surrounded by mountainous terrain, with large payloads [4]. To the authors' knowledge there have been no studies conducted into the three-dimensional analysis of EBF, making the work to be conducted in this study unique. The aim of this study is to obtain pressure distributions over the span of a wing section to allow the determination of increases in lift provided by the use of EBF configuration. Comparisons will be made between the two- and three-dimensional results as well as the spanwise distribution of pressure changes along the wing. The flow over both the two- and three-dimensional wings will be analyzed with and without the engine effects.

The lift and drag values will be required to determine the different values of the lift-to-drag ratio (L/D). The aim is to study a number of different phases of flight with specific attention given to takeoff and landing flight conditions. During each of these stages of flight, the effects of flap deflection will be examined along with the changes of angle of attack that will influence the amount of lift produced and

Received 26 March 2007; revision received 7 June 2007; accepted for publication 17 June 2007.

*Graduate, Aerospace, Mechanical, and Mechatronic Engineering; hamishgriffo@gmail.com. AIAA Member.

†Lecturer; currently Queensland University of Technology, Brisbane, Queensland 4001, Australia; l.gonzalez@qut.edu.au. AIAA Member.

‡Senior Lecturer, Aerospace, Mechanical, and Mechatronic Engineering; ragh@usyd.edu.au.

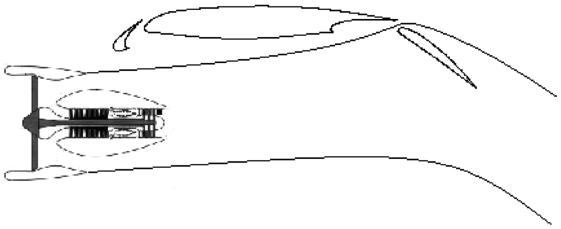

Fig. 1 Externally blown flap.

may have an impact upon the overall change in the L/D ratio [5]. The effect of altering the engine power and hence the speed of exhaust gases will occur by examining the differences of results obtained within the two different flight conditions; takeoff and landing.

II. Methodology

A structured approach was undertaken to ensure that the study advanced in an efficient and productive manner. Once the problem definition, initial research, and tool association had been conducted, validation of the aerofoil chosen [3-element National High-Lift Program (NHLP) [6] laminar flow aerofoil] could be conducted using known wind-tunnel and computational fluid dynamics (CFD) results relating to the NHLP aerofoil. Once suitable results had been obtained, the more challenging prospect of modeling the exhaust gas emissions could begin. This started with the modeling of the engine exhaust flow (Pratt and Whitney PW2000 high-bypass engine was modeled) and incorporating the exhaust flow into the two- and three-dimensional geometries. Analysis was then conducted with and without engine effects allowing for the comparison of two- and three-dimensional results and the changing effects of the engine exhaust flows. Once the comparison of the results was completed, conclusions could be drawn about the increases in lift achieved through the use of EBF over a three-dimensional wing. The primary CFD tools used in this study were the mesh construction tool Gambit and the CFD tool Fluent, both of which are commonly used in aeronautical CFD analysis [7]. All models were constructed using Gambit, with results displayed obtained using the available tools from Fluent. In the case of multiple pressure distribution plots, the numbers obtained from Fluent were overplotted using MATLAB.

A. Geometry

The geometry of the EBF configuration is based upon the published information of the C-17 Globemaster military transport [8]. The location of the engine in relation to the wing, chord size, wing sweep, and taper ratio will all be based upon the C-17 geometry and incorporated into the final EBF configuration. Table 1 provides a summary of the dimensions used in this analysis.[§]

The area of the wing that will be analyzed is that which is most affected by the high-speed flow emanating from the inner engine. This will provide a simulation of flow that is removed from the tip effects of the wing and the influence of the large wing tip. In the two-dimensional case, the engine pylon must be removed to allow flow from the engine to pass through to the wing and no pylon will be included in the three-dimensional case. The reason for emission in three dimensions is that this study is concerned with the effects of high-speed flow interactions with high-lift devices. The effect of the pylon in the flow would be a possible continuation of this study.[¶]

In this case, the authors assumed that the aircraft uses a three-element laminar flow aerofoil, the NHLP aerofoil that has a known geometry with accurate data from both wind-tunnel and CFD analysis which approximates the lifting characteristics of the C-17 aircraft. The standard NHLP aerofoil has a flap deflection of 16 deg. For analysis of the EBF configuration, the flap deflection had to be altered to acceptable limits for the given flight conditions. As a general rule, the flap extension range is up to 40 deg and the useful range for takeoff and landing operations is between a 20 and 40 deg flap deflection. The result of extending the flap into high-speed flow is unknown and beyond the scope of this study, and so it is not possible to define an exact range over which the operation of an EBF system would typically operate. The amount of flap deflection required will be guided by the standard flap deflection used upon transport aircraft. The flap deflection is defined as the number of degrees the flap mean line is offset from the main aerofoil chord line. Because of the nature of the laminar aerofoil, the chord line of the main aerofoil section is assumed to be at an inclination of 0 deg due to the lack of camber present in the main aerofoil.

B. Numerical Implementation

To aid in determining the most accurate results, a number of different turbulence models were examined. The turbulence models which would prove most useful are k-ε, k-ω, Spalart–Allmaras, and Reynolds mean stress (RMS).

The Spalart–Allmaras one-equation turbulence model is an eddy viscosity model where a transport equation is developed based upon dimensional analysis, empiricism, and Galilean invariance [9]. It has been demonstrated by some studies that the Spalart–Allmaras model is useful in accurately predicating flows about multi-element aerofoils, high angles of attack, and aerofoils where boundary-layer separation occurs [10].

The k-ε model is a widely used two-equation eddy viscosity turbulence model. It has been found that the k-ε model suffers in the prediction of transient flows [11]. There have been many variations made to the k-ε model for specific uses. The equation for the k-ε model is not perfect (like most turbulence models) and, for accurate predictions in the immediate vicinity of walls, a very fine mesh is required, especially at high Reynolds numbers [12]. Another shortcoming of the k-ε model is the lack of sensitivity of the model to predict adverse pressure gradients. This causes the prediction of overly high stress levels that causes the delay of, or in some cases prevents completely, the separation of flow.

The k-ω model, like the k-ε model, is a two-equation eddy viscosity turbulence model. The k-ω model is an option available if the more commonly used k-ε model is not suitable. The method of using one equation to model turbulent kinetic energy and the second equation to model the specific turbulent dissipation rate allows a more accurate modeling of adverse pressure gradients than the k-ε model. The k-ω model also has a greater numerical stability compared with most turbulence models. The k-ω model has weaknesses in that the freestream values have a great influence upon the eddy viscosity, and investigation into this effect has found that by using different freestream values, the eddy viscosity can change by an order of magnitude [13].

There are two different methods of predicting turbulent boundary-layer effects. A Reynolds mean stress method or eddy viscosity method can be used. RMS models represent a more accurate method of predicting turbulence, especially under swirling flow conditions or

Table 1 C-17 Globemaster geometry

Aircraft aspect	Value
Wing sweep	25
Wing taper ratio	0.3
Chord at root	14.20 m
Chord at tip	4.29 m
Chord behind inner engine centerline	12.65 m
Chord behind outer engine centerline	7.11 m
Inner engine inlet forward of wing leading edge	1.10 m
Outer engine inlet forward of wing leading edge	1.10 m
Inner engine centerline below wing	2.25 m
Outer engine centerline below wing	2.25 m
Inner engine centerline to fuselage centerline	7.44 m
Inner engine centerline above ground	3.72
Outer engine centerline above ground	3.36 m
Outer engine centerline to fuselage centerline	13.94 m

[§]C-17 Globemaster III dimensions, http://www.globemaster.de/c-17/dimensions.html.

[¶]NASA contributions to the C-17 Globemaster III, http://www.nasa.gov/centers/langley/news/factsheets/C-17.html.

flow over steep curves. However, due to the large amount of computing power required to use this type of model, it is only used when examination of nonisotropic components is important. The eddy viscosity method uses mean flow qualities to represent boundary layer turbulence which requires less computing power compared with the RMS method. A drawback of this method is that the prediction of normal fluid stress is not accurate [14].

1. *Exhaust Gas Properties*

The C-17 Globemaster currently uses the Pratt and Whitney PW2040 (military designation F117-PW100) turbofan engine. In accordance with the use of C-17 geometry, the PW2040 engine will be approximated and produce similar results to the actual engine in use with the current EBF system. The exact engine properties could not be obtained. This means that the fluid properties of the high-speed exhaust emissions of the jet engine must be calculated using the known properties of the engine and applying ideal cycle analysis for a turbofan jet engine. From the properties of the PW2040 engine [15], an ideal cycle analysis can be performed to determine fluid properties of both the core and bypass flow at specific engine settings. The properties that are required to model the exhaust flow in the CFD analysis [16] are U_9, T_9, $U_{9'}$, $T_{9'}$, and the inlet mass flow rate. These flow properties are required for a variety of engine settings depending upon the flight condition to be examined (takeoff or landing). The flow conditions will be determined for the engine at settings of 100, 50, 40, and 30%. For a power setting of 100%, the inlet flow condition is known and the outlet flow properties can be calculated. These settings are indicated in Table 2.

2. *CFD Settings*

The geometry of the two-dimensional EBF configuration incorporates the NHLP aerofoil with the PW2040 engine. A rectangular domain encompasses the EBF geometry. The basic mesh construction for the three-dimensional case is very similar to the mesh used in the two-dimensional case with a few notable differences. The domain is the same size with the exception of the width (10 m) of which the wing spans the entire distance to eliminate tip effects. The dimensions and boundary conditions are summarized in Table 3.

Because of memory allocation limits within Gambit,** a structured grid was used to ensure the maximum cell limit was not exceeded. This had no significant effect upon the results or grid. An unstructured grid would have been implemented if memory constraints had not existed. Because of time constraints, the initial grid sizes were increased and, from previous studies conducted in regard to this issue, a detriment in accuracy was not observed when used in conjunction with grid adaptation. The sizing functions used are summarized in Table 4. Figure 2 shows the mesh on the high-lift devices. The domain size was limited principally by computing power available and time constraints. A comparison was made using a larger domain (length 100 m, height 60 m) to determine whether errors existed in the use of the smaller domain. The larger domain required a significant amount of time to solve and was not suitable for use within the time limitations placed upon this work. The results had only minor differences in the case examined and were considered sufficiently accurate to implement the smaller domain.

3. *Solver Settings*

The solver settings to be used within Fluent have been gathered from previous studies conducted into the NHLP aerofoil and engine flow and refined to provide optimal solver settings in both accuracy and computational time. The final solver settings to be used are summarized in Table 5.

The settings and flow properties were chosen based upon previous studies conducted with the geometry reference values used to calculate the lift and drag coefficients. The energy equation was implemented due to the different temperature gas emanating from the engine exhaust and the requirement to model this interaction. To improve accuracy, grid adaptation using velocity gradient adaptation will be used to increase the accuracy of the flow in areas of high-velocity changes and hence improve overall results. To reduce computational time, an initial residual of 1×10^{-4} will be used and then velocity grid adaptation used and the analysis run again. The grid will continue to be adapted until a value of Y^+/Y^* less than 800 is achieved. The analysis will then be undertaken once finally with a lower residual of 1×10^{-5} to further improve the accuracy. This method will provide an accurate prediction of the flow. The underrelaxation values had to be altered, as some problems occurred to pressure divergence in both the two- and three-dimensional cases, although greater problems were experienced in the three-dimensional case possibly due to the axial flow that existed. The velocity inlet boundary conditions for freestream flow altered the angle of the flow depending upon the angle of attack that was to be examined. The high-speed exhaust flow emanating from the core and bypass velocity inlet boundary conditions was always normal to the inlet surface.

Table 2 Exhaust gas properties

Engine condition	Flow velocity	Flow temperature	Mass flow rate
Takeoff 100%			
Core	583 m/s	561.3 K	608 kg/s
Bypass	321.7 m/s	315.6 K	——
Landing 50%			
Core	536.9 m/s	546.3 K	419 kg/s
Bypass	195.5 m/s	305.1 K	
Landing 40%			
Core	527.0 m/s	543.2 K	381 kg/s
Bypass	170.9 m/s	303.5 K	
Landing 30%			
Core	518.8 m/s	540.7 K	343 kg/s
Bypass	161.5 m/s	301.7 K	

C. Validation

The purpose of the validation process is to determine the accuracy of the model using known wind-tunnel tests with no engine effects present and to compare the two- and three-dimensional results obtained when the engine effects are implemented. This allows for a greater confidence in the results obtained.

1. *Without Engine Effects*

The three-dimensional wing section was placed in a domain where the span of the wing section is the same as the span of the test domain that will produce results similar to the results obtained in a two-dimensional wind-tunnel analysis. The same settings used in Fluent and Gambit for the two-dimensional analysis will be used in the three-dimensional analysis. Figure 3 demonstrates the differences found when using a three-dimensional model compared with when a two-dimensional analysis was conducted. Included are results from a previous CFD/wind-tunnel study of the pressure distribution over the NHLP aerofoil [17]. The previous study involved an analysis of the NHLP aerofoil using CFD and wind-tunnel techniques. The data obtained in this pervious study has been taken and compared with results of the two-dimensional CFD analysis done in this study to aid in the validation and confidence of the pressure distributions obtained. A significant proportion of the study, which is used to validate the results in Fig. 3, is concerned with the position of the boundary-layer transition. This effect is difficult to model using turbulence models and was found to be especially difficult to predict over the slat. There is a possibility of an error in modeling the small wake flow emanating from the slat which affects the flow over the leading edge of the main aerofoil section due to difficulties with the position of the boundary-layer transition.

There are small differences in the results, most notably the higher pressure coefficient obtained near the leading edge of the main aerofoil section (in the three-dimensional analysis). This is most

**Fluent, Inc., Gambit release notes (version 2.3.16), April 2006; available from http://fluent.com.

Table 3 Aerofoil geometry and domain boundary conditions

Dimensions		Boundary conditions	
Chord at root	14.20 m	sides	symmetry
Chord at tip	11.10 m	inlet	velocity inlet (domain flow conditions)
Wing sweep	25 deg	outlet	pressure outlet
Taper ratio	0.33	top	velocity inlet (domain flow conditions)
Wing span	10 m	bottom	velocity inlet (domain flow conditions)
Wing area	114.5 m^2	slat	wall
Engine location (in relation to leading edge of aerofoil)	engine inlet 1.10 m forward	main aerofoil	wall
		flap	wall
	engine centerline 2.25 below	engine inlet	wall
Rectangular domain	width 70 m (aerofoil offset 20 m forward)	engine	wall
	height 40 m	bypass	velocity inlet (bypass flow conditions)
		core	velocity inlet (core flow conditions)

Table 4 Sizing functions

	Sizing function	
Slat	start size	0.01
	grid limit	0.5
	growth rate	1.1
Main aerofoil	start size	0.02
	grid limit	0.5
	growth rate	1.2
Flap	start size	0.01
	grid limit	0.5
	growth rate	1.1
Engine	start size	0.02
	grid limit	1.1
	growth rate	0.5

likely the result from the mixing of the flow that is possible in three-dimensional analysis, yet not so in the two-dimensional analysis. The mixing of the three-dimensional flow leads to a slight increase in boundary-layer thickness and slightly greater separation, which in turn leads to a small reduction in the calculated pressure coefficient and hence a reduction in lift. The observation of the spanwise distribution of the pressure coefficient shows a very uniform pressure distribution. This is the expected result, as testing a three-dimensional aerofoil which spans the entire width of the test area should produce results similar to a two-dimensional test and would be considered a pseudo-two-dimensional test in a physical wind tunnel. The existence of wall conditions in the vicinity of the edges of the aerofoil could also lead to a small reduction in overall lift, however, very few edge effects are observed. No three-dimensional tip effects are sought or observed in the analysis due to the aerofoil spanning the entire width of the test area and are not examined as tip effects do not impact this area of study. The EBF configuration is positioned a significant distance inboard of the wing tips so that tip effects will have no noticeable effect upon the flow in the vicinity of the EBF [18].

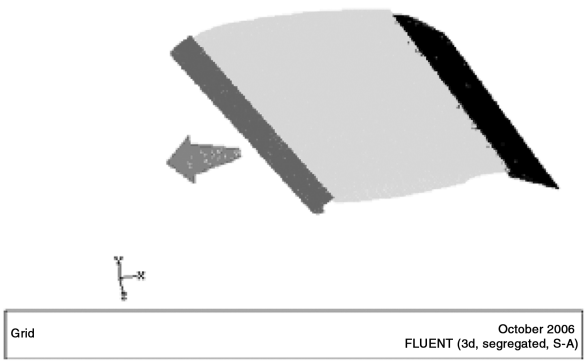

Fig. 2 EBF configuration (three-dimensional).

2. With Engine Effects

In the following sections, the flow will be validated between two and three dimensions in the vicinity of the slat, main aerofoil section, and flap. This can be done as the two-dimensional flow will approximate the flow in three dimensions directly behind the engine centerline with no axial mixing. This is not an ideal case for use as a comparison as there are differences expected in the flow. This comparison is used to observe if the flow patterns directly behind the engine centerline in the three-dimensional results are similar to the two-dimensional results. An amount of correlation is expected and this will increase the confidence of the three-dimensional results. As there are no other studies using a similar geometry and aerofoil that examine the externally blown flap configuration in either wind-tunnel or CFD analysis, this was the best way of increasing confidence in the data obtained in the three-dimensional analysis.

A flap deflection of 30 deg and angle of attack of 0 deg is used with power settings of 100 and 40% analyzed. There is only a minor variation in the flow around the slat. The two- and three-dimensional results are very similar and changes produced do not incorporate a significant change in lift. From observations made of the pressure distribution over the main aerofoil section, it can be seen that there is no major effect on the flow over the main aerofoil caused by the differences in flow around the slat. From contour plots, it can be seen that the spanwise changes occurring in the flow around the slat are not significant. Similar to the results obtained from the validation with no engine effects, the results obtained comparing the two- and three-dimensional flow over the flap and main aerofoil section have a similar "shape." The three-dimensional results are generally the same or slightly lower in magnitude compared with the two-dimensional results (see Fig. 4). This reduction is expected for the same reason given in Sec. II.C.1 and has a greater impact when the engine effects are analyzed. The ability of the flow to mix in an axial manner will reduce the overall three-dimensional effect and is observed in the general drop in magnitude of pressure on both the flap and main aerofoil. The flow around the slat does not follow this pattern, the reason being that the high-speed flow does not directly impact upon the flow around the slat [19]. Thus, the three-dimensional flow results can be said to be sufficiently accurate as they closely resemble the two-dimensional results.

III. Two-Dimensional Analysis

The two-dimensional results obtained are shown in Table 6 and demonstrate the change in lift and drag that occurs behind the engine centerline. For the majority of the cases without power, the L/D ratio

Table 5 Fluent solver settings and flow properties

Solver settings		Flow properties	
Turbulence model	Spalart–Allmaras	density	1.1767 kg/m^3
Equations	segregated implicit	freestream Mach number	0.18
Energy equation	included	freestream temperature	288 K
Density	ideal gas (compressible)	freestream pressure	101.3 kPa
Initial residual (all equations)	1×10^{-4}	viscosity	1.789×10^{-5}
Final residual (all equations)	1×10^{-5}	Re[a]	49.9×10^6

[a]Characteristic length used for Re is the average chord of the test section.

decreases when flap deflection increases, and the lift coefficient increases with an increase in angle of attack. There is a significant increase in lift when power is applied with a corresponding rise in drag. There is a large decrease in the L/D ratio when the EBF configuration is analyzed with different power settings (100, 50, 40, 30%), which indicates that there is a greater increase in drag relative to the lift increases observed. The decrease in the L/D ratio is expected due to the interactions of the high-speed exhaust flow with the extended flap and leads to greater inefficiencies during periods of flight when the flaps are extended. The comparatively large drag increase indicates that more engine power will be required to overcome the loss created by transferring some of the thrust to lift (and hence causing more drag) through the EBF configuration. There is a small drop in the L/D ratio when the engine power is reduced (50, 40, 30%) compared with the full power case.

The two-dimensional results obtained simulate the flow behind the engine centerline and the EBF effect will be reduced in the spanwise direction away from the engine centerline. This will be more evident in the three-dimensional analysis. The effect of changes of engine power, flap deflection, and angle of attack will be examined in two dimensions using pressure coefficient distribution plots over the slat, main aerofoil, and flap (all sections combined on a single plot with slat covering 0–1.5 m, main aerofoil covering 1.5–9.7 m, and flap covering 9.7–12.3 m) combined with selected velocity contour plots.

A. Effect of High-Speed Exhaust

There is a significant difference between the flow encountered with engine effects and without engine effects. The result is a large change in the amount of lift produced. To analyze the effect of engine power on the flow, a flap deflection of 30 deg will be used with an angle of attack of 0 deg. The situation without engine effects, full power, and reduced (40%) power will be discussed. There is a noticeable effect upon the main aerofoil section and the flap pressure distribution that is caused by the high-speed exhaust gas from the engine. A comparison can be made between the three engine cases: no power, full power (100%), and landing power (40%), and very different flow patterns develop. Overall, the flow with full power produces a high-velocity stream of air that partially mixes before it comes into contact with the aerofoil. The high-velocity air is drawn upward toward the bottom surface of the aerofoil. This is caused by the low-pressure air that lies above the wing and the tendency of the higher pressure air below the wing to flow through the gap between the main aerofoil and the flap [20]. If the engine power is reduced and hence the high-speed air slows, the rise is much greater, which aids in offsetting the lift lost by reducing engine power (see Fig. 5).

The effect of decreasing the engine power, and hence allowing the high-speed velocity air to rise, can be seen on the pressure distribution for the lower surface of the main aerofoil section. There is almost no change in pressure coefficient distribution on the top surface of the main aerofoil; this is shown by the velocity flow contours. On the bottom surface, a region of relatively low-pressure area exists forward of the contact area between aerofoil surface and the high-speed flow. This can clearly be seen in the pressure distribution on the bottom surface and is very pronounced when the power is set at 40%. This is followed by a significant increase in pressure when the high-speed flow impacts the bottom surface of the aerofoil. The result of this is a large increase in lift due to the large increase in pressure on the lower surface of the aerofoil. From the pressure distribution shown in Fig. 6, it can be seen that the increase in lift produced by the main aerofoil section is approximately equal for both full power and reduced power. This is counterintuitive and an unexpected result. The significant point to be made is that reducing engine power will not result in a correspondingly equal loss of lift increase. This phenomenon of increase in lift due to the upward-moving, high-speed flow occurs often throughout this study.

The flow around the slat changes in no significant way when an engine is present. The slat is too far above and forward of the engine for any influence of the high-speed exhaust to have a marked effect. A small difference in pressure distribution is noticed, however, this is caused more by the existence of the physical engine in the flow rather than the exhaust that emanates from it. The flow around the slat in the velocity contour plots, shown in Fig. 5, demonstrates what has been determined from the pressure distribution. Both plots are very

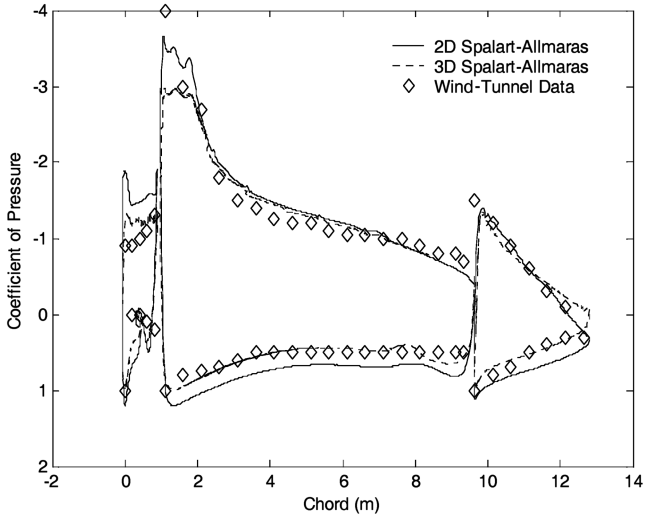

Fig. 3 Main aerofoil C_p distribution (without engine effects).

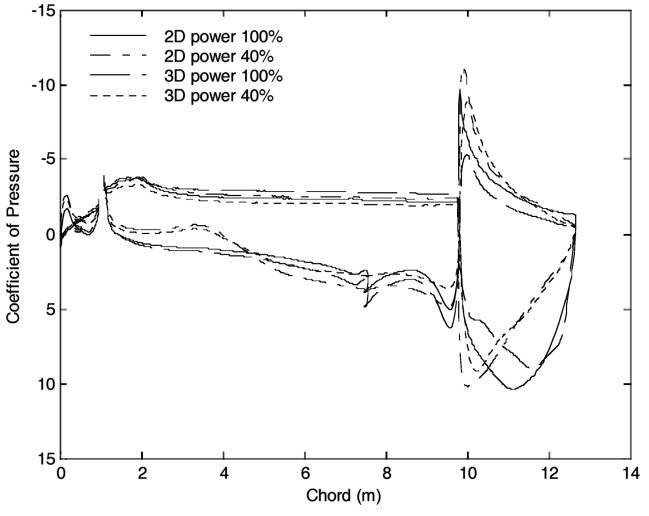

Fig. 4 Main aerofoil C_p distribution (with engine effects).

Table 6 Two-dimensional lift and drag results

	C_L	C_D	L/D
No power			
Flap 20 deg, α 0 deg	1.377	0.057	24.184
Flap 20 deg, α 10 deg	2.361	0.126	18.683
Flap 30 deg, α 0 deg	1.586	0.084	18.785
Flap 30 deg, α 10 deg	2.458	0.162	15.161
Flap 35 deg, α 0 deg	1.312	0.132	9.919
Flap 35 deg, α 10 deg	2.192	0.196	11.202
Takeoff (100% power)			
Flap 20 deg, α 0 deg	3.541	0.511	6.934
Flap 20 deg, α 10 deg	5.910	1.495	3.953
Flap 30 deg, α 0 deg	5.665	0.965	5.871
Flap 30 deg, α 10 deg	7.559	2.309	3.273
Landing (40% power)			
Flap 30 deg, α 0 deg	5.088	0.782	6.502
Flap 30 deg, α 10 deg	5.896	2.069	2.849
Flap 35 deg, α 0 deg	7.749	1.657	4.677
Flap 35 deg, α 10 deg	8.323	2.736	3.042
Landing (30% power)			
Flap 30 deg, α 0 deg	5.045	0.759	6.649
Flap 30 deg, α 10 deg	5.767	2.006	2.874
Flap 35 deg, α 0 deg	7.579	1.603	4.727
Flap 35 deg, α 10 deg	8.129	2.647	3.072
Landing (50% power)			
Flap 30 deg, α 0 deg	5.036	0.835	6.033
Flap 30 deg, α 10 deg	6.168	2.184	2.825
Flap 35 deg, α 0 deg	8.010	1.737	4.611
Flap 35 deg, α 10 deg	8.650	2.888	2.996

similar, with differences occurring in the freestream flow caused by the physical presence of the engine. The other difference is the more aligned flow in the case in which full power is applied behind the slat and under the main aerofoil. This is caused by the engine exhaust and influences the flow behind, but has very little influence upon the flow through the slat.

The flow around the flap changes dramatically with the high-speed interaction from the engine and is a major focus of the study. Before the high-speed flow is introduced, a large amount of separation can be observed on the trailing upper surface of the flap in Fig. 5. This leads to a reduction in lift produced by the flap [21]. When the high-speed flow is introduced, there is virtually no separation zone behind the flap. Separation is removed because the high-speed flow has sufficient energy to remain attached to the flap until the trailing edge [22]. The high-speed air flows through the gap between the flap and main aerofoil, drawn there by the low-pressure conditions that exist on the top surface of the aerofoil. The flap increases the amount of lift produced in two ways. The speed of flow over the top surface of the flap is increased and pressure is reduced, while the high-speed flow impacts the lower surface of the flap and significantly increases the pressure. This can clearly be seen from the pressure coefficient distribution shown in Fig. 6.

There is a difference between the full-power and reduced-power exhaust that affects the flow on both the upper and lower surface of the flap. Pressure is found to be lower on the upper surface of the flap which is counterintuitive. This is a flow on effect of the larger rise toward the main aerofoil explained earlier. This greater rise allows

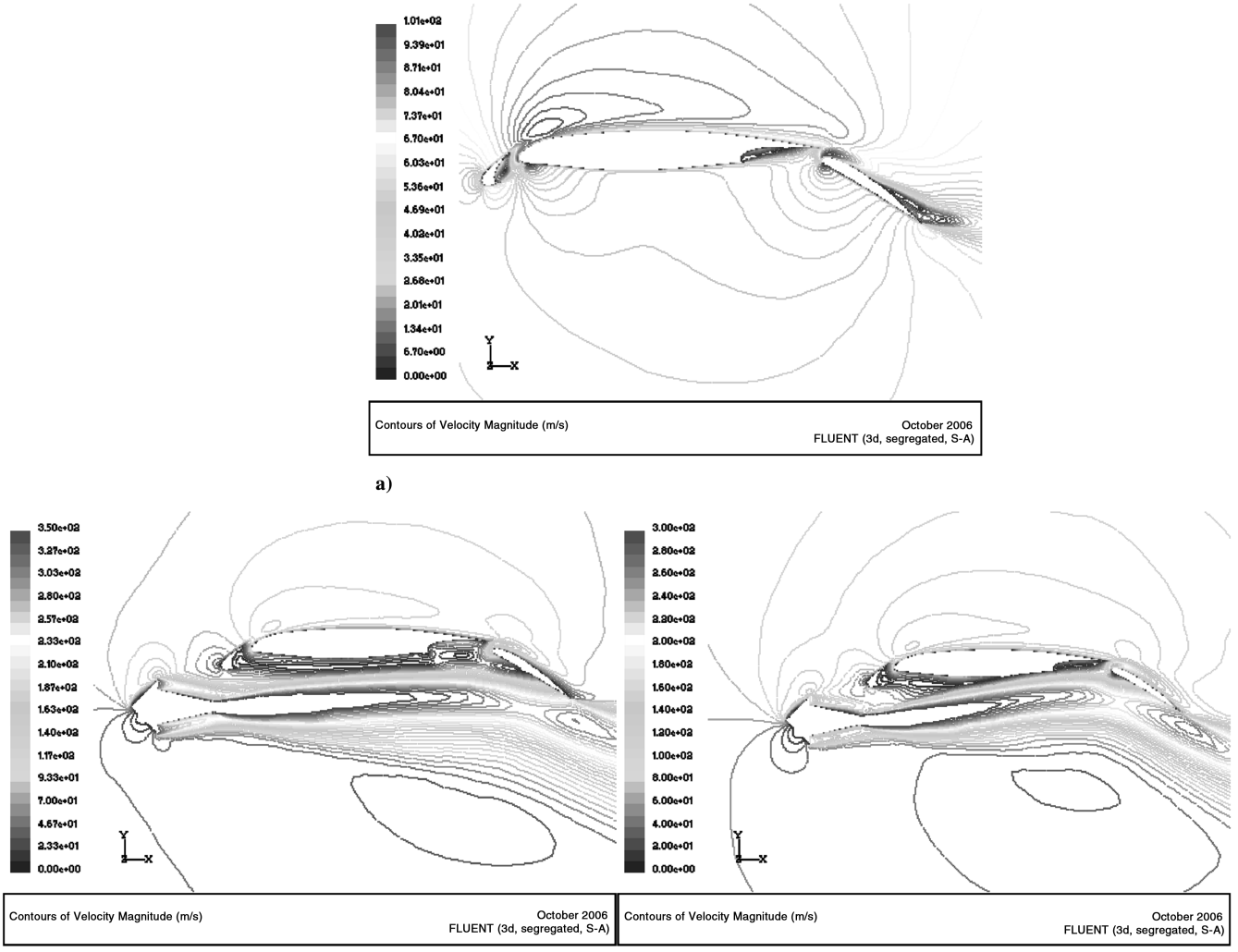

Fig. 5 Velocity contour plot, flap 30 deg, $\alpha = 0$ deg: a) without power, b) power 100%, c) power 40%.

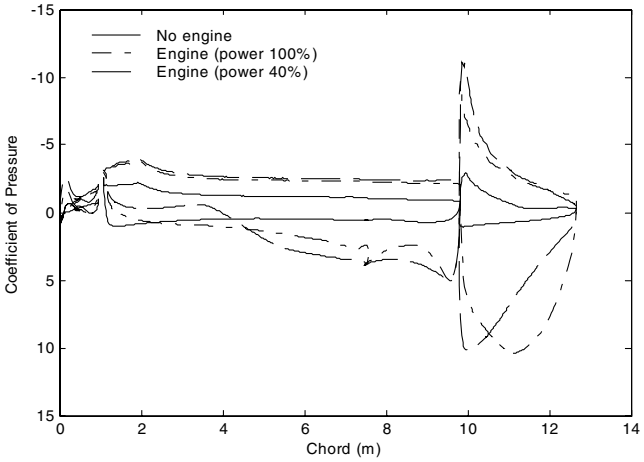

Fig. 6 Pressure coefficient distribution, flap 30 deg, $\alpha = 0$ deg.

the highly energized exhaust gas to have a greater effect on the upper surface of the flap, where the flow on the flap upper surface is actually faster despite a lower power setting. The difference is only slight and occurs only on the forward third of the flap; the rest of the pressure distribution is equal. A large difference is noticed on the lower surface of the flap. When full power is applied, there is a large pressure increase on the lower surface that covers the lower half of the flap. This can be seen from both pressure coefficient distributions and the velocity contour plot (Figs. 5 and 6) where there exists an area of low-speed flow in the middle of the flap. The same pattern is noticed when a lower power setting is applied. This maximum pressure occurs nearer the leading edge of the bottom surface of the flap and drops steadily. This is a direct effect of the higher speed flow impacting the flap and causing very high pressure. The high-pressure area is lower on the flap when full power is applied due to the previously discussed bending of high-velocity flow.

B. Effect of Flap Deflection

There are multiple flap deflections that can be used in the EBF configuration. Three flap settings are used in this study: 20, 30, and 35 deg. All flap deflections have been tested at full power and the two larger flap settings have been tested at reduced (40%) power. The effect of changing the flap setting with a constant angle of attack (0 deg) and constant power settings (100%) will be discussed. As discovered before, the change in flow around the slat is minimal, as can be seen from the velocity contour plot shown in Fig. 7. Altering the flap deflection has an impact on the flow on both the upper and lower surface of the main aerofoil section. The increase of flap deflection causes a uniform decrease in pressure on the upper main aerofoil. There is no indication from the pressure or velocity plots that this decrease in pressure is greatly changed by the engine (see Fig. 7). From the previous section on engine effects it is reasonable to conclude that this change in pressure is due primarily to the flap deflection increasing the speed over the top of the aerofoil. Significant changes are noticed on the lower surface which can be attributed to a combination of engine and flap effects. The pressure increases as the flap deflection increases. The 20 and 30 deg deflections produce a similar result with a uniform change in pressure. The 35 deg flap deflection deviates from this pattern and produces a very different pressure distribution compared with the previous two flap deflections. This is caused by the further lowering of pressure on the upper surface of the aerofoil, causing the high-speed flow from the engine to rise and impact the lower surface of the aerofoil. This greatly increases the amount of lift produced and has implications for flow over the flap.

The flow over the flap has no uniformity between any of the flap deflections, which can be seen in Fig. 8. The flow over the top of the flap increases in speed and hence a lower pressure occurs as the flap deflection is further increased producing an increase in lift. This has been compounded with the rising of the high-speed flow which occurs with an increase in flap deflection. Noticeable separation occurs on the upper surface of the 35° deg deflected flap causing a sudden increase in pressure. This has been caused by the higher deflection of the flap. It was also found that reducing the deflection of the flap will increase the pressure on the upper surface.

It may be possible to reshape the flap to reduce the separation and maintain the low-pressure and hence further increase the effectiveness of the blown flaps [23]. There is no separation at either of the lower deflections and a steady pressure distribution is observed. There is a general increase in pressure on the lower surface of the flap. The rising of the high-speed flow again causes this, and the subsequent highest pressure point illustrates this. The greater the deflection, the greater the rise of high-speed air and hence the further forward the highest pressure point will be. This situation holds true and is easily observable from pressure and velocity contour plots. The higher the flow rises, the greater the volume of high-speed flow that requires deflection, hence the higher the pressure. Also holding true is the fact that as flap deflection increases so does maximum pressure.

When power was reduced and the flap deflection increased, the pressure distribution significantly decreased on the leading lower surface and increased on the trailing lower surface of the main aerofoil. This is an extreme condition of combining the effects of lowering the engine power and increasing flap deflection. The slower speed exhaust and lower upper-surface pressure cause a larger rise

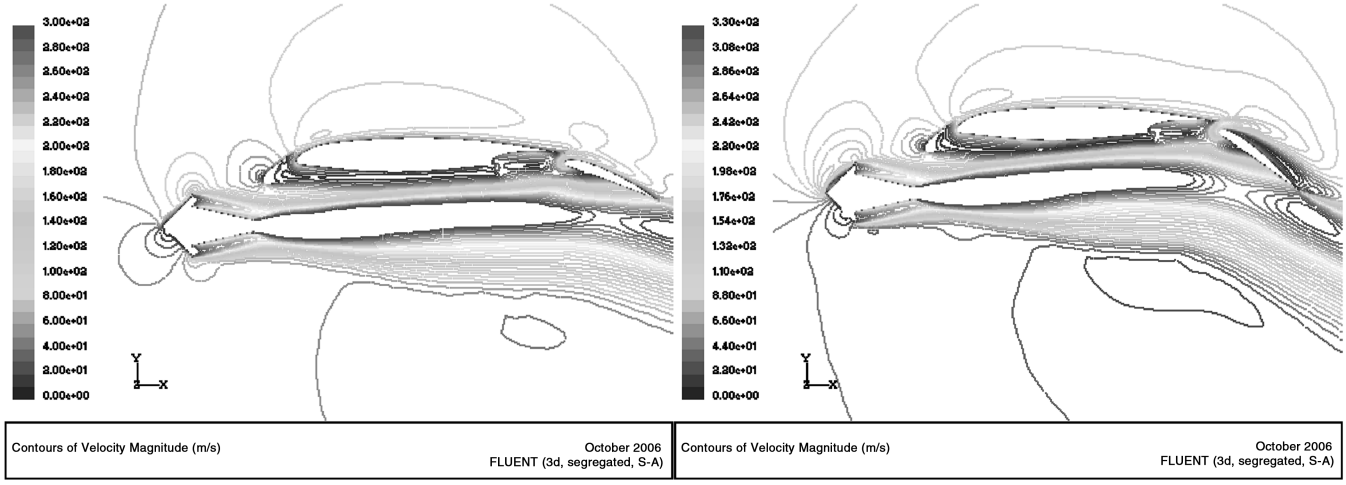

a) b)

Fig. 7 Velocity contour plot, power 100%, $\alpha = 0$ deg: a) flap 20 deg, b) flap 35 deg.

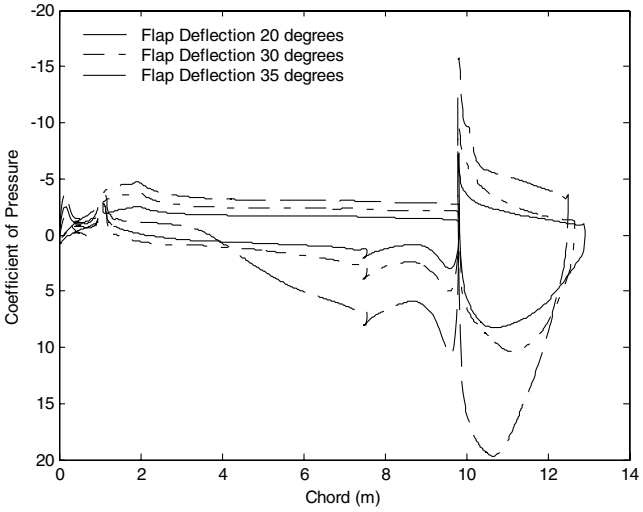

Fig. 8 Main aerofoil pressure coefficient distribution, power 100%, $\alpha = 0$ deg.

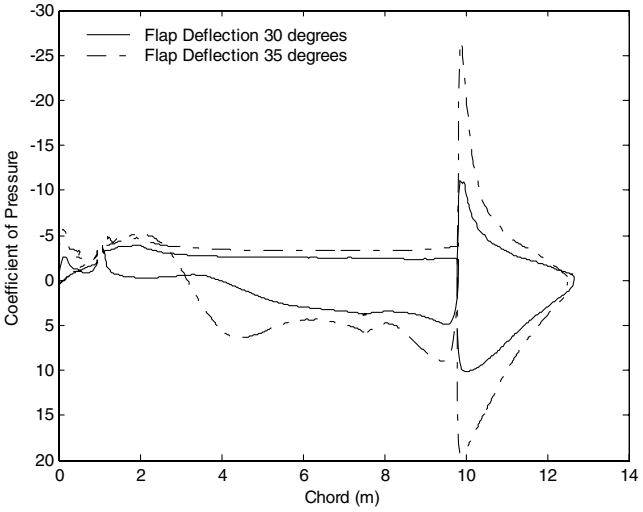

Fig. 9 Pressure coefficient distribution, power 40%, $\alpha = 0$ deg.

and produce these results. The pressure coefficient distribution demonstrates very well the effect of this on the lower surface of the aerofoil shown in Fig. 9.

C. Effect of Angle of Attack

The effect of angle of attack will be analyzed by comparing flow at an angle of attack of 0 deg to an angle of attack of 10 deg. Changes in flap deflection will also be included to note whether there exists any unexpected results based upon the work done comparing flap deflection and engine power changes on the flow. Increasing the angle of attack causes a uniform decrease in average pressure throughout the slat. There is no indication that the engine has a large effect upon the flow. The change in flap deflection has only a limited effect. The flow around the slat is affected to a significant amount only by a change on angle of attack. This is expected as the changes in flap deflection and engine power are too far removed from the slat to have a significant direct impact. The change provides a general increase in lift from the slat consistent with an increase in angle of attack. The corresponding flow patterns on the upper main aerofoil are more significant and are partially the result of the decrease in pressure through the slat.

The increase in angle of attack alters the flow on the top and bottom of the aerofoil and alters the manner in which the engine exhaust flows toward the aerofoil (see Fig. 10). The lower pressure will further aid in drawing the high-speed flow toward the aerofoil and the impact of the freestream velocity will add to this effect. When full power is applied, a pressure increase is experienced similar to those previously observed when the flap was deflected or power reduced (see Fig. 11). If a combination of these effects are implemented, the effect is built upon. Observing the lower surface pressure distribution, it is seen that at reduced power (40%), high angle of attack, and high flap deflection (35 deg), the engine flow contacts the aerofoil very quickly and stabilizes until the flap insert where the pressure further decreases. The pressure distribution fluctuates enormously and it is possible that more lift is produced at lower angles of attack with the same flap deflection and reduced power setting. This requires further analysis. Significant separation is observed when a high flap deflection with reduced power occurs with a loss of lift experienced.

As previously mentioned, separation begins to occur on the leading top surface of the flap causing an increase in pressure and loss of lift. The increase in angle of attack brings the point of highest pressure forward on the bottom of the flap, creating a linear decay of pressure to the trailing edge. This is caused by the further raising of the high-speed flow caused both by the freestream flow, which is at an angle to the exhaust flow, and the further decrease in pressure on the top surface of the aerofoil caused by increasing the angle of attack, as seen in Figs. 10 and 11.

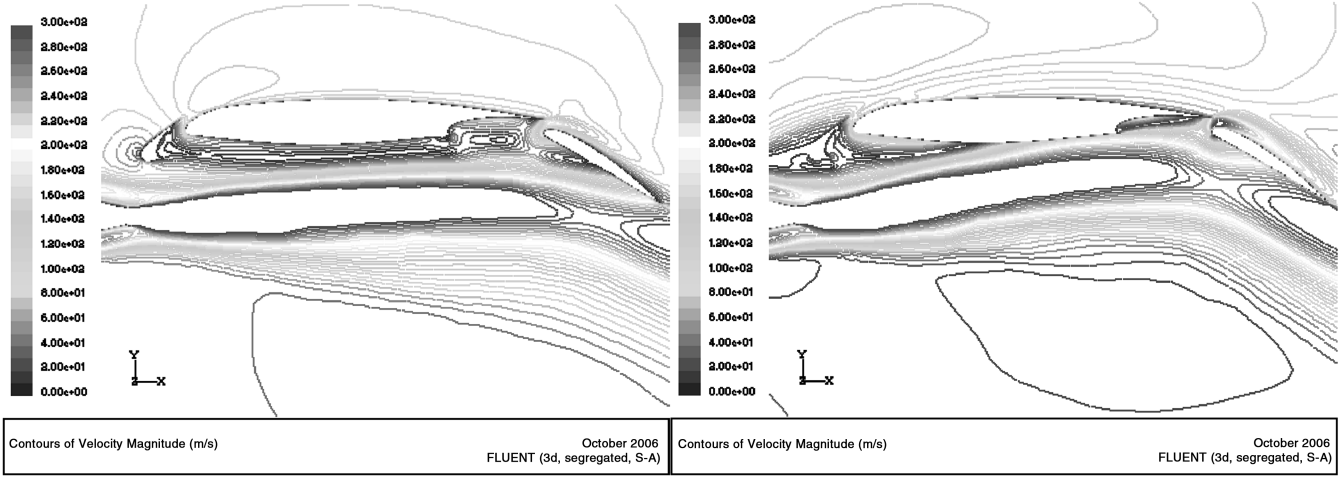

a) **b)**

Fig. 10 Velocity contour plot, power 100%, Flap 30 deg: a) $\alpha = 0$ deg, b) $\alpha = 10$ deg.

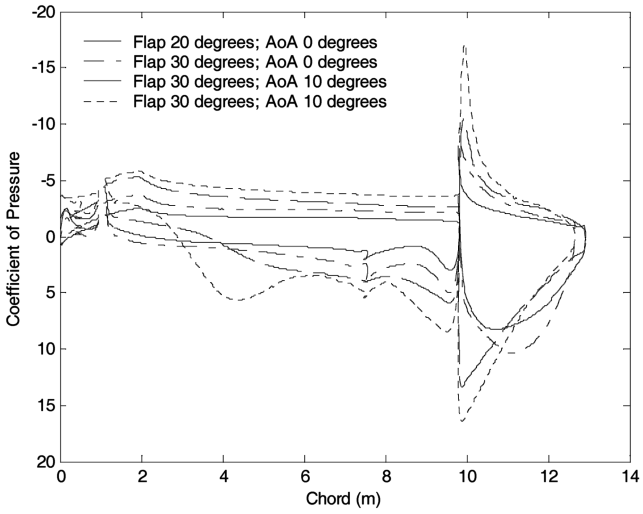

Fig. 11 Main aerofoil pressure distribution; power 100%.

IV. Three-Dimensional Analysis

Results for the lift coefficients and lift-to-drag ratio are listed in Table 7 and consist of three sections: lift and drag with engine effects (takeoff 100%, landing 40%) and without engine effects (no power), lift and drag of the entire wing, and lift and drag directly behind the width of the engine. From the changes in lift and drag, it can be seen that the majority of the lift and drag changes emanate from directly behind the engine and this will be examined in detail in the next section. From comparisons between the C_L values obtained for the total wing and directly behind the engine, it is clear that the majority of the increase in lift occurs in close vicinity of the engine. A very important effect is that a reduced lift increase is observed when the two-dimensional results are compared. The lift increase in the two-dimensional analysis indicated that a large lift increase would be expected, however, this is not the case due to the reduced effect of the EBF as the spanwise distance away from the engine increases. The percentage changes between the two- and three-dimensional analyses are covered in Sec. V.

The drag increases relative to lift as engine power and flap deflection increase, and hence the L/D ratio decreases. The decrease in L/D observed is greatest directly behind the engine, however, the true effect is only observed when the change over the entire wing is calculated. There still exists a large drop in the L/D ratio, however, the ratio is significantly greater than the two-dimensional results. This is expected, as the EBF effect reduces as distance increases from the engine centerline. The reduced L/D ratio indicates that more thrust will be required, which is the direct cause of using a powered lift augmentation system such as EBF and the combining effect of the increase in drag caused by this method of lift augmentation.

Pressure coefficient distribution plots (similar to those in the two-dimensional analysis) are examined at both the engine centerline and at the engine boundary to allow observation of the reduced effect of the high-speed exhaust gases as spanwise distance increases. Selected pressure contours surface plots demonstrate the changes in pressure distribution on the lower surface of the wing.

A. Effect of High-Speed Exhaust on Spanwise Flow Distribution

The effect of the engine on spanwise flow distribution is observed by changing the engine power and keeping the flap (30 deg) and angle of attack (0 deg) constant. The flow over the main aerofoil section is not significantly influenced by the high-speed flow out near the engine boundary. The high-speed flow does not rise sufficiently enough to have a large impact upon the flow over the bottom surface of the flap and combines to uniformly increase the pressure on the top surface of the aerofoil. This does not indicate that there are no engine effects on the engine boundary. Because of the diffusion of the flow, some effect will occur and this can be seen by the slightly greater pressure magnitude obtained compared with the no engine pressure distribution.

Figures 12 and 13 show that a noticeable change in pressure distribution occurs over the flap. This can be seen not only in the pressure distribution, see Fig. 12, but also from the contour surface plot, see Fig. 13. The change in pressure distribution on both upper and lower surfaces of the flap is of a similar shape, however, the most important aspect is the symmetry of the pressure distribution in the spanwise direction. The symmetry indicates the flow has no tendency to "slide" up or down the wing in a spanwise direction. This was observed in cases with no engine effects when the angle of attack was altered. The change in lift across the wing is symmetrical, allowing a linear lift prediction for this case between two and three dimensions for the current geometry and engine type [24].

B. Effect of Flap Deflection

By maintaining full power, a constant angle of attack, and altering the flap deflection, the spanwise flow distribution can be found by comparing the pressure distributions behind the centerline and at the engine boundary. The effect on the main aerofoil can be clearly seen with a uniform increase in pressure on the upper surface of the main aerofoil as distance from the engine centerline increases. On the bottom surface of the aerofoil, the large pressure change recorded has disappeared at the edge of the engine effect seen in Fig. 14. The high-speed exhaust is still having a limited impact upon the flow on the bottom side of the aerofoil.

There is still a notable difference in the flow over the flap with the flap deflection having a noticeable effect on the spanwise flow

Table 7 Three-dimensional EBF results

	Three-dimensional (total)			Three-dimensional (behind engine)		
	C_L	C_D	L/D	C_L	C_D	L/D
			No power			
Flap 20 deg, α 0 deg	1.309	0.059	22.031	——	——	——
Flap 20 deg, α 10 deg	2.070	0.164	12.627	——	——	——
Flap 30 deg, α 0 deg	1.547	0.089	17.405	——	——	——
Flap 30 deg, α 10 deg	2.205	0.235	9.380	——	——	——
Flap 35 deg, α 0 deg	1.250	0.129	9.708	——	——	——
Flap 35 deg, α 10 deg	1.825	0.173	10.572	——	——	——
			Takeoff (100% power)			
Flap 20 deg, α 0 deg	1.399	0.100	14.057	1.631	0.193	8.454
Flap 20 deg, α 10 deg	2.528	0.311	8.138	2.878	0.555	5.191
Flap 30 deg, α 0 deg	2.131	0.227	9.373	2.395	0.595	4.026
Flap 30 deg, α 10 deg	3.250	0.502	6.469	3.954	1.166	3.392
			Landing (40% power)			
Flap 30 deg, α 0 deg	1.869	0.141	13.232	2.075	0.335	6.189
Flap 30 deg, α 10 deg	2.645	0.418	6.326	3.026	0.681	4.445
Flap 35 deg, α 0 deg	2.860	0.263	10.874	3.151	0.761	4.141
Flap 35 deg, α 10 deg	3.088	0.446	6.923	3.890	1.226	3.173

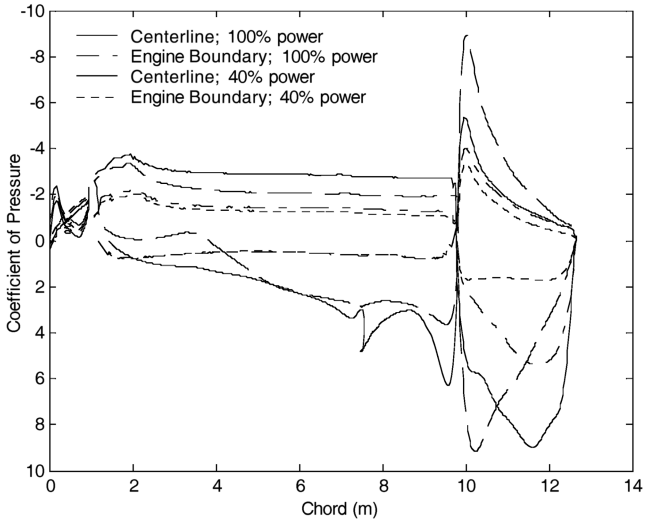

Fig. 12 Main aerofoil spanwise pressure coefficient distribution, flap 30 deg, $\alpha = 0$ deg.

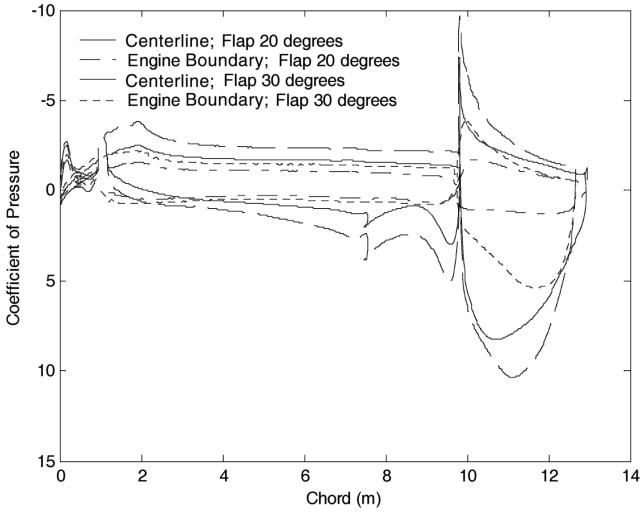

Fig. 14 Pressure coefficient distributions, 100% power.

distribution. When the flap angle is only 20 deg, there are no significant engine effects on either the top or bottom surface of the flap. When the flap is deflected 30 deg, there is still a large engine effect. This can be seen on both the upper and lower surfaces and it is much more noticeable on the lower surface as shown in Fig. 15. There is a low-pressure region on the upper leading edge of the flap. The separation that has been observed previously along with a steep increase in pressure is not present. The characteristic high-pressure region on the bottom surface of the flap is clearly visible and the high-pressure location is further back on the flap than at the centerline and less intensive. From the contour plots, the same conclusion can be reached. There is a residual spreading of high-pressure on the lower surface of the flap when the deflection is 30 deg, which does not occur for the lower flap deflection. The low-pressure region and its spanwise distribution can also be observed again with the high flap deflection promoting the low-pressure area to remain intensive and hence increasing overall lift. The pressure change caused by the reduced effect of the high-speed flow is generally symmetrical on either side of the engine centerline.

The reason this occurs is due to the lower pressure produced when a high flap deflection occurs. This phenomenon has been covered in the two-dimensional analysis. This pressure distribution ensures that the flow out near the engine boundary is still drawn up to have a noticeable effect on the aerofoil. The greater flap deflection also lowers the flap further in the flow (in the vertical direction) requiring the high-speed flow to rise less to have an impact upon the flap.

C. Effect of Angle of Attack

To analyze the effect of angle of attack on spanwise flow distribution, the angle of attack was increased to 10 deg while the flap angle remained at 30 deg and power held at 100%. The flow condition on the main aerofoil resembles the results obtained on the main aerofoil section when altering the flap deflection. The high-speed flow has no major impact upon the flow over the main aerofoil near the engine boundary. The increase in angle of attack causes no noticeable pressure changes on the lower or upper surface of the main aerofoil section seen in Fig. 16.

Although the decrease in pressure caused by a higher angle of attack causes significant effects in the area around the engine centerline, the flow is not affected near the engine boundary. The effect on the flap is again only marginal with no significant difference between 0 and 10 deg angle of attack. The pressure distributions obtained do not display the entire situation. From the pressure contour plots shown in Fig. 17, it can clearly be seen that the pressure distributions tend to slide toward the tip of the wing. As there are no wing tip effects and this situation occurs only when the angle of attack is increased, one can conclude that this is caused by the increased angle of attack. This has implications for the overall lift of the wing. It appears that the increase in angle of attack has caused the overall flow and, with it, the engine effects to slide down the wing. This same condition was observed when the angle of attack was increased when there was no engine effect. It appears likely that this is caused in part by the sweep and taper of the wing. The pressure distribution observed in this case further confirms the observations

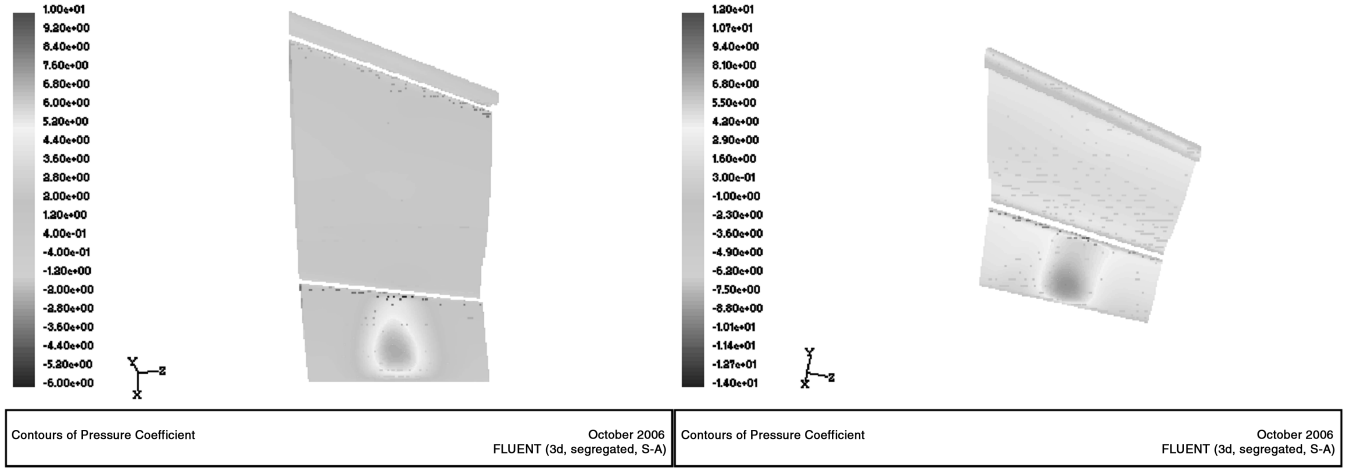

a) b)

Fig. 13 Spanwise pressure contour (lower surface), flap 30 deg, $\alpha = 0$ deg: a) without engine, b) power 100%.

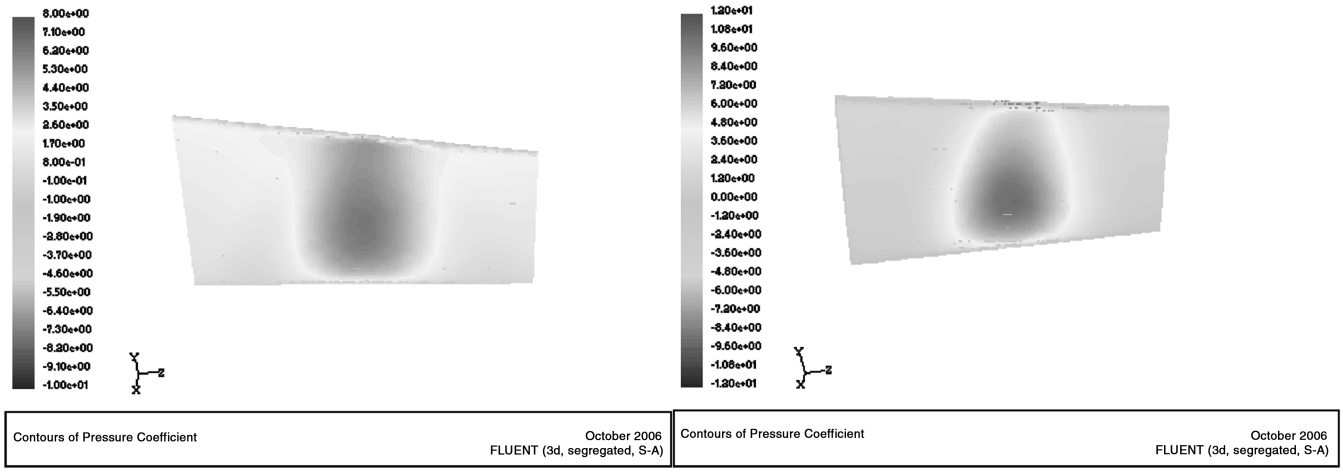

a) b)

Fig. 15 Flap (lower surface) spanwise pressure contour, power 100%, $\alpha = 0$ deg: a) flap 20 deg, b) flap 30 deg.

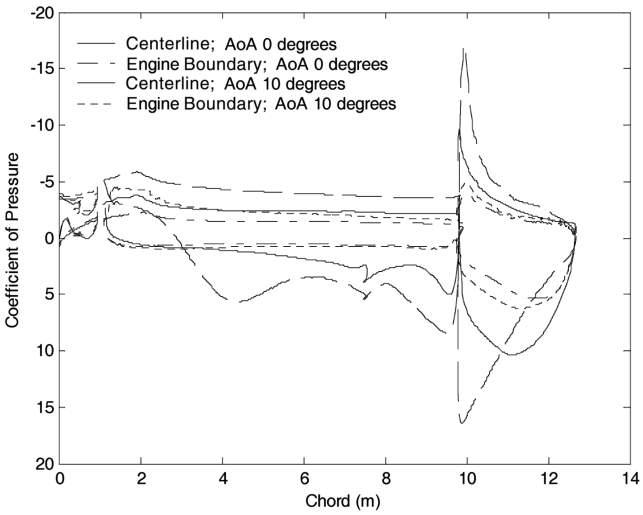

Fig. 16 Pressure coefficient distribution, engine 100%, Flap 30 deg.

previously made with an increase in the angle of attack. The same flow pattern is noticed on the upper and lower surface of the flap.

The significant differences in symmetry of spanwise flow will have an impact on attempting to calculate a relationship between two-dimensional lift increases and three-dimensional lift increases. A relatively symmetrical pressure distribution was observed with engine and flap deflection changes which did not hold true for changes in the angle of attack.

V. Discussion of Two- and Three-Dimensional Results

As stated in the previous section, there is a symmetrical pressure distribution for both engine and flap deflection changes that allows for an assumption of linearity between the results. When the angle of attack was altered, the spanwise pressure distribution changed in a significant way. The pressure distribution was no longer symmetrical, leading to a change in the total lift produced along the span of the aerofoil. Because of the linear relationship found with engine changes and flap deflection, there is an indication that a unique relationship exists for changes of angle of attack between two- and three-dimensional lift increases.

The relationship could prove very useful in the design of aircraft incorporating externally blown flaps. If it is possible to create a model that allows the prediction of three-dimensional results from simple two-dimensional analysis, it would be possible to quickly examine a number of different configurations in two dimensions before the detailed analysis was undertaken. This would allow savings in both time and money during the project. There remain

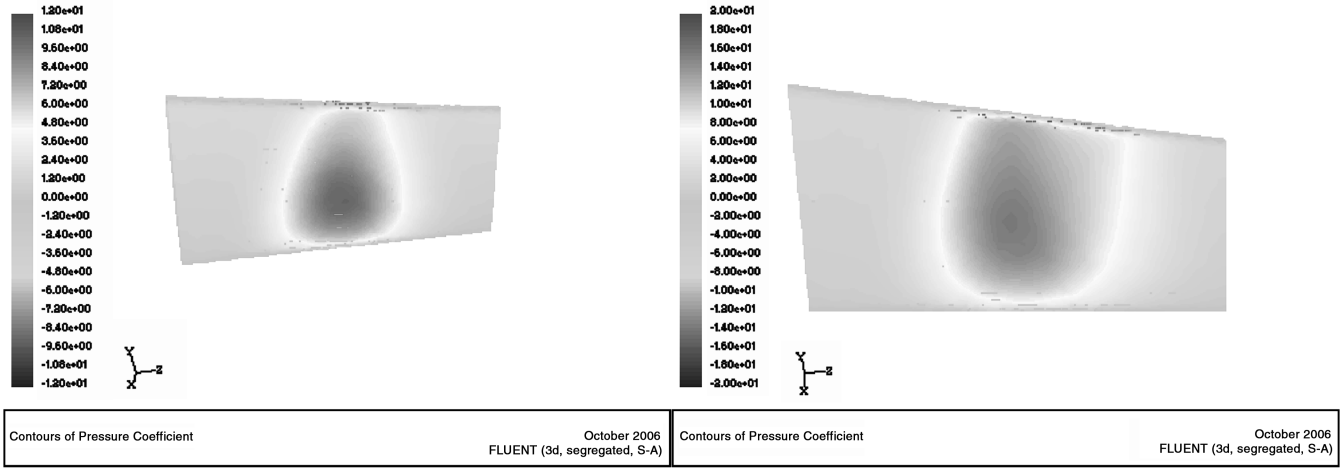

a) b)

Fig. 17 Flap (lower surface) spanwise pressure contour, power 100%, flap 30 deg: a) $\alpha = 0$ deg, b) $\alpha = 10$ deg.

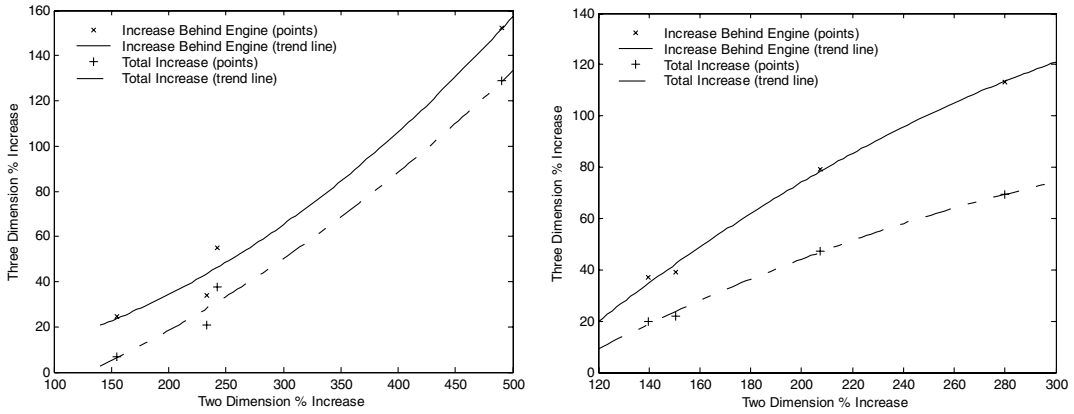

Fig. 18 Two- and three-dimensional percentage increase relationship: a) $\alpha = 0$ deg, b) $\alpha = 10$ deg.

problems in using such a model, including the unknown effect of altering the geometry of the aerofoil and the limitation that the current analysis takes no wing tip effects into account. A greater number of cases need be analyzed to gain a firm understanding of the model, as well as analysis at differing angles of attack and using different aerofoil geometries. Despite these problems, there are gains to be made from creating such models that would allow optimization of the design to occur at greater efficiency.

Using the available data, a second-order model has been created for the test cases available. The percentage lift increases have been plotted in Fig. 18 for angle of attack of 0 and 10 deg, and a trend between the points can clearly be seen. This same trend does not exist if different angles of attack are plotted on the same figure; the trend is unique for each angle of attack. Two sets of points are plotted and related to the two-dimensional increase: the three-dimensional percentage increase directly behind the engine, and the three-dimensional percentage increase excluding the area of the wing directly behind the engine. This was done to improve the accuracy of the predictive equations that were developed. A second-order least-squares approximation was made to create a line of best fit between the data points. There are not enough data points to obtain an accurate comprehensive trend line that would allow predictions of three-dimensional lift from two-dimensional results, only a general trend which invites further study. The data obtained can be used only for the same aerofoil geometry and the equations will only be applied if the increase in lift falls between the recorded data.

The effectiveness of EBF will decrease as the span of the wing increases. It has been found that the majority of the increase in the lift provided by the high-speed flow emanating from the engine occurs over the diameter of the engine exhaust area. This can be seen by comparing the relative percentage increases for the two-dimensional aerofoil with the three-dimensional wing shown in Table 8. Further examination of the spanwise flow distribution conducted in Sec. IV demonstrates that the pressure changes, and hence the lift changes are reduced significantly at the engine boundary, leading to the conclusion that the vast majority of increase in lift occurs in close proximity to the engine centerline. This concept is supported by the two-dimensional data that model the flow directly behind the engine data and for which lift increases have also been obtained. Comparing the two- and three-dimensional results show that the lift increase found in the two-dimensional case is higher than the overall lift increase behind the entire engine. The effectiveness of the EBF depends greatly upon the ratio between the span and engine diameter. A constant engine diameter and span were used in the geometry in this analysis. If the assumption is made that the flow characteristics would change in a linear manner when span is altered, a relationship between the lift increase for a given span can be obtained. This is a rough guide based on the results achieved with the given geometry and allows the estimation of the effect of altering the span if the remaining geometry was kept constant.

The alteration of the diameter of the engine will affect the span-to-engine ratio and hence influence the amount of lift an EBF configuration would produce. Different engine geometries were not used in this study, and so there can be no estimate of the effect of changing the diameter of the engine in affecting the overall lift. This is because altering the engine diameter may affect the flow through

Table 8 Percentage Increase found using EBF

	C_L values			C_L percentage increase		
	Two dimensional	Three dimensional, total	Three dimensional, engine	Two dimensional	Three dimensional, engine	Three dimensional, total
Takeoff (100% power)						
Flap 20 deg, α 0 deg	3.541	1.399	1.631	155.2	24.6	6.9
Flap 20 deg, α 10 deg	5.910	2.528	2.878	150.3	39.0	22.1
Flap 30 deg, α 0 deg	5.236	2.131	2.395	242.5	54.8	37.8
Flap 30 deg, α 10 deg	7.559	3.250	3.954	207.5	79.3	47.4
Landing (40% power)						
Flap 30 deg, α 0 deg	5.088	1.869	2.075	232.9	34.1	20.8
Flap 30 deg, α 10 deg	5.896	2.645	3.026	139.9	37.2	20.0
Flap 35 deg, α 0 deg	7.749	2.860	3.151	490.6	152.1	128.8
Flap 35 deg, α 10 deg	8.323	3.088	3.890	279.7	113.2	69.2

the wing and would undoubtedly be combined with different exhaust velocities and temperatures. For this reason, only the change in lift due to span can be estimated, not the change due to engine diameter, and hence the span-to-engine diameter ratio cannot be used.

Many of the statements that have been made regarding the increase in lift hold true for a corresponding increase in drag. There is no incentive to create an efficient wing during the flight stage in which the EBF will be used, as efficiency is required during the sections of the flight in which a clean configuration is used. Drag values have been listed to demonstrate that although drag increases it does not become excessive. If the drag became too high, then the benefits of the EBF would be neutralized by the excessive engine power required. The decrease in L/D ratio is expected as a reduction is observed when high-lift devices are used [25]. From the results, there is sufficient engine power to overcome the increase in drag caused by implementing the EBF configuration.

Although not as effective as the two-dimensional results estimate, there is no doubt that a significant increase in lift is experienced when an EBF is implemented. This increase in lift will provide improved performance during the critical flight stages of takeoff and landing.

VI. Conclusions

The aim of this study was to determine the effectiveness of three-dimensional EBF and compare them to the results obtained from a two-dimensional study. This has been achieved and it was found that the effect of EBF is reduced as the span of a wing is increased. Despite this decrease, large increases in the amount of lift produced were still observed, demonstrating that the use of EBF does have the ability to significantly improve performance in the takeoff and landing flight conditions with no detrimental effect upon the efficiency of the wing in clean configuration. The key element, the rising of the high-speed exhaust flow, was observed and the impact of this on the lower surface of the aerofoil was noted. The rising high-speed flow aids in improving the effectiveness of EBF as engine power decreases so that the loss of lift observed due to reducing power is not as great. This was uniformly observed in the spanwise distribution of the flow. This study has demonstrated the different effects of EBF on three- and two-dimensional geometries and found a relationship between the lift increases for unique angles of attack. The relationship developed is unique to the geometry used in this study and leads to further work whereby the relationship is known, allowing the expansion of the predictive equations to incorporate different geometries and allow successful design and implementation of EBF using basic two-dimensional results. This study has opened up avenues for further inquiry. Such areas include the investigation into engine variation, optimized flow over the flap to prevent separation at high flap deflections, and the effect of multiple engines. The area of EBF has only recently come into use in a production model aircraft and the effects observed from the performance of the C-17 have been impressive. The results of this study confirm the advantages of the EBF configuration for practical use, and this study, combined with the extension work indicated, could aid in expanding the understanding and use of EBF and the subsequent improvements in aircraft performance.

References

[1] Crouch, T. D., *Wings: A History of Aviation from Kites to the Space Age*, Norton, New York, 2004.

[2] Roe, M. H., Renselaer, D. J., and Quam, R. A., *STOL Tactical Aircraft Investigation, Externally Blown Flap*, Rockwell International, Los Angeles, 1973.

[3] Washington, H. P., and Gibbons, J. T., "Analytical Study of Takeoff and Landing Performance for a Jet STOL Transport Configuration with Full-Span Externally Blown Triple-Slotted Flaps," NASA TR D-7441, Oct. 1973.

[4] Globemaster III Background, Boeing, St. Louis, MO, 2006, http://www.boeing.com/defense-space/military/c17/docs/C-17_overview.pdf.

[5] Korbacher, G. K., Aerodynamics of Powered High-Lift Systems, *Annual Review of Fluid Mechanics*, Vol. 6, Jan. 1974, pp. 319–358.

[6] DeRango, S., *Higher-Order Spatial Discretization for Turbulent Aerodynamic Flows*, Univ. of Toronto, Toronto, 2001.

[7] Chi, X., Zhu, B., Shih, T., I-P., Addy, H. E., and Choo, Y. K., CFD Analysis of the Aerodynamics of a Business-Jet Aerofoil with Leading-Edge Ice Accretion, *42nd Aerospace Sciences Meeting and Exhibit*, AIAA 2004-0560, 2004.

[8] C-17 Globemaster III, *All the World's Aircraft*, Edited by P. Jackson, Jane's Information Group, Alexandria, VA, 2006.

[9] Rudman, M., One-Equation Turbulence Model For Generalized Newtonian Fluid Flow, Thesis, William Marsh Rice University, Houston, TX, July 2003.

[10] Pan, J., Loth, E., and Bragg, M. B., RANS Simulations of Aerofoils with Ice Shapes, *AIAA 41st Conference*, AIAA 2003-0729, 2003.

[11] Tanner, F. X., Zhu, G.-S., and Reitx, R. D., A Turbulence Dissipation Correction to the k-epsilon Model and its Effects on Turbulence Length Scales in Engine Flows, *International Multidisciplinary Engine Modeling User's Group Meeting at SAE Congress*, March 2001.

[12] Turbulence Modelling, Part 2: Limitations of k-epsilon Model, QNET CFD, Luzern, May 2002, www.qnet-cfd.net.

[13] Menter, F. R., "Improved Two-Equation k-omega Turbulence Models for Aerodynamic Flows," NASA TM 103975, Oct. 1992.

[14] Davidson, L., *An Introduction to Turbulence Models*, Chalmers Univ. of Technology, Göteborg, Sweden, Nov. 2003.

[15] Aero-Engines, *All the World's Engines*, Edited by M. Daly, Jane's Information Group, Alexandria, VA, 2006, Pratt and Whitney PW2000 series.

[16] Slater, J. W., *Supersonic Axisymmetrical Jet Flow: Study #2*, NASA Lewis Research Center, Cleveland, OH, Nov. 1998.

[17] Morrison, J. H., Numerical Study of Turbulence Model Predictions for the MD30P/30N and NHLP-2D Three-Element High-Lift Configurations, NASA Scientific and Technical Information Office, Hanover, MD, Dec. 1998.

[18] Montoya, L. C., "Effect of Winglets on a First-Generation Jet Transport Wing,Part 3: Pressure and Spanwise Load Distribution for Semi-Span Model at Mach 0.30," NASA TR D-8478, June 1977.

[19] Smith, C. C., "Effect of Engine Position and High-Lift Devices on Aerodynamic Characteristics of an Externally-Blown Flap Jet STOL Model," NASA TR D-6222, March 1971.

[20] Graebel, W. P., *Engineering Fluid Mechanics*, Taylor and Francis, London, 2001.

[21] Bertin, J. J., *Aerodynamics for Engineers*, 4th ed., Prentice–Hall, Upper Saddle River, NJ, 2002.

[22] Petrov, A. V., Aerodynamics of Aircraft with Wing-Powered Lift Systems, *International Powered Lift Conference*, AIAA 1993-4386, 1993.

[23] Mendenhall, M. R., and Spangler, S. B., "Calculations of the Longitudinal Aerodynamic Characteristics of Upper-Surface-Blown Wing-Flap Configurations," NASA TR NAS1-14086, 1978.

[24] Mason, W. H., Subsonic Aerodynamics of Airfoils and Wings, Aerospace and Ocean Engineering, *Configuration Aerodynamics*, Dept. of Aerospace and Ocean Engineering, Virginia Polytechnic Inst. and State Univ., Blacksburg, VA, Chap. 6, April 2006.

[25] Abbott, H., and Von Doenhoff, A. E., *Theory of Wing Sections*, Dover, New York, 1959.